



Geophysical Research Letters°

RESEARCH LETTER

10.1029/2021GL096478

Key Points:

- Ray tracing under a minimum-B pocket geometry for chorus waves is conducted
- Under average hot electron condition, MBPG chorus waves get damped within 1 or 2 Re of distance and thus are highly localized
- Even when the hot electron proportion is only several ten thousands, MBPG chorus waves are very unlikely to propagate into the plasmapause

Correspondence to:

N. Kang, nkang20@atmos.ucla.edu

Citation:

Kang, N., Bortnik, J., An, X., & Claudepierre, S. G. (2021). Propagation of chorus waves generated in Minimum-B pockets. *Geophysical Research Letters*, 48, e2021GL096478. https://doi.org/10.1029/2021GL096478

Received 5 OCT 2021 Accepted 29 NOV 2021

Author Contributions:

Conceptualization: Jacob Bortnik
Formal analysis: Ning Kang
Funding acquisition: Jacob Bortnik, Xin
An, Seth G. Claudepierre
Investigation: Ning Kang, Jacob Bortnik,
Xin An, Seth G. Claudepierre
Methodology: Ning Kang
Project Administration: Jacob Bortnik
Supervision: Jacob Bortnik
Validation: Ning Kang
Visualization: Ning Kang
Writing – original draft: Ning Kang
Writing – review & editing: Ning
Kang, Jacob Bortnik, Xin An, Seth G.
Claudepierre

© 2021. American Geophysical Union. All Rights Reserved.

Propagation of Chorus Waves Generated in Minimum-B Pockets

Ning Kang¹, Jacob Bortnik¹, Xin An², and Seth G. Claudepierre¹

¹Department of Atmospheric and Oceanic Sciences, University of California, Los Angeles, CA, USA, ²Department of Earth, Planetary, and Space Sciences, University of California, Los Angeles, CA, USA

Abstract We present the first ray tracing results of chorus waves generated in minimum-B pockets. A new ray tracer is developed to accommodate an arbitrary magnetic field model, which enables us to construct minimum-B pocket geometries using the Tsyganenko (1989) model. Rays with different frequencies and initial wave normal angles are launched from minimum-B pockets and traced under different geomagnetic activity and hot electron density conditions. Our results indicate that chorus waves generated from minimum-B pockets are usually highly localized and thus are unlikely to be detected unless the spacecraft is very close to the source region. These waves are also very unlikely to propagate into the plasmasphere. The propagation distances generally decrease with increasing geomagnetic activity.

Plain Language Summary Chorus waves are an important kind of electromagnetic waves in the near-Earth environment. We trace the ray paths of chorus waves generated in regions of low magnetic field intensity in the high-latitude dayside magnetosphere (referred to as minimum-B pockets) using a newly developed ray tracer which can deal with more complex geomagnetic field than the simplest model of magnetic field produced by a dipole magnet. Rays are launched with a range of frequencies, initial wave normal angles and space weather conditions. Our results indicate that chorus waves generated from minimum-B pockets are usually highly localized and thus are very unlikely to be detected unless the spacecraft is very close to the source region. They are also very unlikely to propagate into the plasmasphere. The propagation distances in general decrease with enhanced geomagnetic activity.

1. Introduction

Chorus waves are intense, whistler-mode electromagnetic emissions frequently observed in the Earth's magneto-sphere (e.g., Burtis & Helliwell, 1969; Li et al., 2009). Chorus waves are believed to be a very important electron accelerator and are a main source of relativistic electrons in the Earth's outer radiation belt due to their wave-particle interactions with electrons (e.g., Gołkowski et al., 2019; Horne & Thorne, 2003; Summers et al., 1998; Thorne et al., 2013). It is generally accepted that the equatorial region outside the plasmapause is the main source region of chorus waves (LeDocq, et al., 1998; Santolik et al., 2003), but it has also been proposed that the region of minimum magnetic field intensity (minimum-B pocket) could potentially be an important high latitude chorus wave source region in the outer dayside magnetosphere (Tsurutani & Smith, 1977). However, due to a lack of in situ spacecraft observations in the high-latitude, high-L-shell minimum-B pocket regions, there are very few observations of minimum-B pocket generated (MBPG) chorus waves (e.g., Vaivads et al., 2007). Thus, we have very little knowledge of the propagation characteristics of the MBPG chorus waves. For instance, it is currently not well understood how far these MBPG waves can propagate from their source region, how long they survive before being damped, and what regions they can potentially propagate into. The goal of the present study is to address these questions.

The ray tracing technique is an approach that has been extensively used to study plasma wave propagation in the near-Earth space environment (Bortnik, Inan, & Bell, 2003a, 2003b; Horne, 1989; Inan & Bell., 1977; Kimura, 1966). Previous ray tracers have dealt predominantly with dipole fields (e.g., Horne & Thorne, 1993; Inan & Bell., 1977) or quasi-dipole fields (Yue et al., 2017), thus generally being unable to model the minimum-B pocket structures. In this work, we successfully employ a non-dipole field, the Tsyganenko 1989 (T89) model, to a newly developed ray tracer, and study the propagation of MBPG chorus waves.

KANG ET AL.



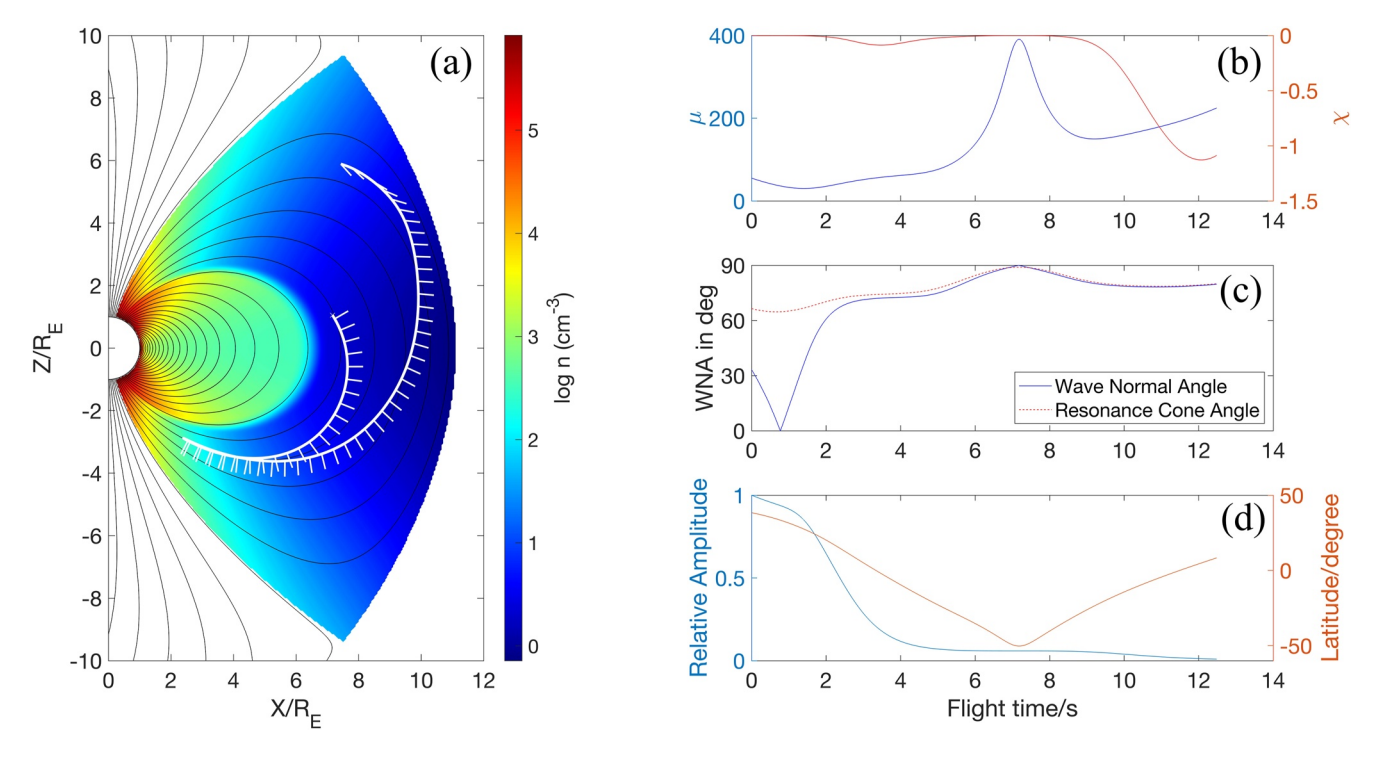


Figure 1. Example of one single ray. The model is Kp = 1, $L_{pp} = 6.3$, and the ray is launched with frequency $0.4f_{ce}$ and initial WNA 147° . (a) Trajectory of the ray. The thick white line is the trajectory, and the thin short white lines attached to the trajectory marks the direction of wave vectors there. The background contour is the electron density, and black lines are the field lines. (b) The refractive index of the ray vs. flight time. The blue line is the real part of the refractive index, and the red line imaginary part. (c) WNA of the ray vs. flight time. The red dashed line is the local resonance cone angle. (d) Relative amplitude and latitude of the ray vs. flight time.

2. Model

We use a newly developed Python-based ray tracer, PyRay, to investigate the propagation of chorus waves originating in minimum-B pockets. The PyRay code is designed for cold plasma ray tracing with the ability to accommodate arbitrary magnetic field models. Hamilton's equations are used to advance the rays following Haselgrove (1954), in which we set ϕ (the azimuthal angle) and v^{ϕ} (ϕ component of the reflective index vector) to 0 to simplify the equations and reduce the computations to a 2D geometry. The cold plasma dispersion relation is obtained from the well-known Stix equations (Equations 29–35, Stix, 1992), in which the effects of multiple species of heavy ions are included. A damping module independent of the main ray tracer is included into the code. Given a hot electron distribution, the damping rate is calculated using the method of Brinca (1972), similar to previous studies (Bortnik et al., 2003a, 2003b, 2007, 2008).

2.1. Magnetic Field Model

The geometry of magnetic field is reflected in the spatial variation of gyrofrequency Ω_e and the wave normal angle θ , which is embedded into the cold plasma reflective index, thus influencing the Hamiltonian which drives the rays. Therefore, an arbitrary magnetic field model can be adopted so long as the magnetic vector at each location in the domain $\boldsymbol{B}(\boldsymbol{r})$ is smooth and well defined everywhere so that Ω_e and θ (and their spatial derivatives) can be calculated. In this work we use a simple but realistic T89 model (Tsyganenko, 1989), which takes only the geomagnetic Kp index as its model input. In this study we use two Kp values to specify the T89 magnetic field: Kp = 1 representing quiet times, and Kp = 4 representing geomagnetically active times. The field lines for the Kp = 1 model are shown in Figure 1a as black solid lines. We can see clear minimum-B pockets at high latitudes of L shell 8–10 (e.g., near the location where the ray is launched).

KANG ET AL. 2 of 8



2.2. Density Model

The diffusive equilibrium (DE) model (Angerami & Thomas, 1964) has been widely used to describe the spatial distribution of plasma density in ray tracing programs (e.g., Bortnik et al., 2003a, 2003b; Horne, 1989; Kimura, 1966). However, the DE model relies on a dipole field geometry and is thus not directly applicable in our study. To construct a more realistic density distribution, we apply the DE model only to the equator to obtain an equatorial electron density $n_{e_{eq}}(r)$, and assume an ionospheric electron density at the Earth surface given by:

$$n_{e_{\text{iono}}}(\lambda) = 10^6 \text{ cos } \lambda \text{ cm}^{-3},$$
 (1)

where λ is the magnetic latitude. For off-equatorial regions, we assume that on each field line, the density increases with latitude as:

$$n_{e_{\text{line}}}(\lambda) = \frac{n_0}{\cos^m \lambda},\tag{2}$$

where n_0 and m are free parameters to be determined, following previous similar fits (Denton et al., 2002, 2006). Specifically, for any point (r, λ) , we perform a bi-directional field line tracing starting from this point. In one direction the field line crosses the equator at altitude r_{eq} , and in another direction field line intersects the ionosphere at latitude λ_{iono} . Using these two conditions, n_0 and m can be solved for as:

$$\begin{cases}
n_0 = n_{e_{eq}}(r_{eq}) \\
n_{e_{eq}}(r_{eq}) \\
m = \frac{\ln \frac{n_{e_{eq}}(r_{eq})}{n_{e_{iono}}(\lambda_{iono})}}{\ln \cos \lambda_{iono}}
\end{cases}$$
(3)

The equatorial density $n_{\rm eq}(r)$ is set so that at $r = 10R_E$ ($R_E = 6371$ km is the Earth radius), $n_{\rm eeq} \approx 1$ cm⁻³ based on satellite observations (Bortnik et al., 2016).

We use two $n_{\rm e_eq}$ models which differ in the locations of the plasmapause. The parameter $L_{\rm pp}$ that defines the L shell of plasmapause in DE model is chosen to be either 4.5 or 6.3, the former representing the typical location of plasmapause, and the latter a relatively extreme case of a very extended plasmapause, which is typical of the dayside under quiet conditions (Moldwin et al., 2002). The color in Figure 1a shows the electron density distribution for the $L_{\rm pp}=6.3$ density model. Note that this model gives a sufficiently smooth and slow-varying plasma density profile, so that the WKB approximation holds for our ray tracing, and will not come across the small-scale density structures (e.g., Hosseini et al., 2021; Katoh, 2014; Ke et al., 2021; Streltsov et al., 2006; Xu et al., 2020). Due to the nature of our method, density is only defined for closed field lines, which is sufficient for the purposes of the present investigation.

2.3. Hot Electron Model

The hot electron distribution is fitted to the statistical results of Li et al. (2010) for hot electron (E > 100 eV) flux between 4 < L < 10 using THEMIS data. We use the outermost bins at noon in Figure 3 of Li et al. (2010) to accommodate the location of our minimum-B pockets. We follow the fitting method of Bortnik et al. (2007) to arrive at a fitted distribution function:

$$f(v) = 2.52v^{-3.29} \text{cm}^{-3},\tag{4}$$

where v is the electron velocity in unit cm · s⁻¹. This hot electron distribution corresponds to a hot electron (E > 100 eV) total density of ~0.2 cm⁻³, which makes up 2%–10% of total electrons in minimum-B pockets. Such a high proportion of hot electrons leads to strong damping and the rays are expected to be damped out very quickly. Thus, for each model case run with Equation 4, two more cases are run with 10% and 1% hot electrons of Equation 4, to explore the effects of a reduced hot electron density upon wave propagation (see below).

KANG ET AL. 3 of 8



3. Results and Discussion

We use three magnetospheric models representative of different conditions: (1) Kp = 1, L_{pp} = 4.5; (2) Kp = 1, L_{pp} = 6.3; (3) Kp = 4, L_{pp} = 4.5. All rays are launched from the center of the minimum-B pocket, at $r = 9.5R_E$, $\lambda = 38^\circ$ (this location is at the center of a minimum-B pocket for both Kp = 1 and 4 magnetic field geometry). Due to the highly limited spatial scale of chorus source region (LeDocq, et al., 1998; Santolik et al., 2003), we neglect the growth phase of chorus waves and assume waves have already grown to full amplitude within the narrow source region when they are launched. For each magnetospheric model, the rays have three frequency components representative of typical chorus waves: 0.2, 0.4 and 0.6 times of local electron gyrofrequency f_{ce} at the launched point. And for each frequency, 22 rays whose initial wave normal angles (WNAs) are uniformly spaced between the positive and negative local resonance cone angle are traced. That leads to 3 (magnetosphere models) × 3 (hot electron density) × 3 (frequencies) × 22 (initial WNAs)= 594 rays in total. Ray tracing is terminated if the ray is damped to 1% of its initial amplitude ("extinguished"), if the ray propagates out of the closed field line region ("escaped"), or if the ray phase velocity becomes lower than the thermal velocity of electrons with 1 eV temperature ("absorbed"). In the latter case, the chorus wave energy would be absorbed by the thermal plasma because the majority of the cold plasma would look "hot" to the wave and our cold plasma assumption thus breaks down.

Figure 1 shows a typical ray tracing result. The ray propagates in magnetospheric model 2: Kp = 1, $L_{pp} = 6.3$, and has a frequency of $0.4f_{ce}$ and an initial WNA of 147° . The thick white line in Figure 1a represents the ray path, and the thin short white lines around the ray path mark the direction of the local wave vector k along the ray path. The ray experiences a reflection at a lower altitude due to the inclusion of ions, which is consistent with previous whistler wave ray tracing results (e.g., Bortnik et al., 2008; Kimura, 1966). Figure 1b shows the time evolution of the refractive index. We see that $|\chi| \ll \mu$ so the weak damping assumption holds, which assures the validity of our calculation of linear damping rate. Figure 1c is the time evolution of ray WNA. The blue solid line is the WNA and the red dashed line shows the local resonance cone angle for comparison. The ray quickly approaches the local resonance cone angle after launching, and exceeds the local resonance cone angle near the reflection point, which again agrees with previous work (e.g., Bortnik et al., 2003a, 2003b). Figure 1d shows the relative amplitude and the latitude of the ray. The ray eventually is damped to 1% of its initial amplitude, where it is considered to be damped out and the ray tracing is terminated.

Figure 2 compares the ray tracing results in the three magnetospheric models. The left column (Figures 2a, 2d and 2g) corresponds to model 1 (Kp = 1, $L_{pp} = 4.5$), the middle column (Figures 2b, 2e and 2h) corresponds to model 2 (Kp = 1, $L_{pp} = 6.3$), and the right column (Figures 2c, 2f and 2i) corresponds to model 3 (Kp = 4, $L_{pp} = 4.5$). From top to bottom, the three rows correspond to rays with frequencies 0.2, 0.4 and 0.6 f_{ce} , respectively. In each subplot, the color of the ray represents the initial WNA. On each ray are three markers marking the terminating points of the rays. The triangle marker is for hot electron distribution corresponding to (Equation 4), the circle marker for 10% reduced hot electron distribution, and the star marker 1% reduced.

In the left and the middle columns we see that all the triangle markers are very close to the injection point, which means that under average hot electron flux conditions derived from the statistical results of Li et al., (2010), MBPG chorus waves do not propagate far and are highly localized to the minimum-B pockets. Two ray paths that experience reflection are emphasized by thick lines in Figure 2a. The orange line is reflected outward (to larger L-shells) while the green one is reflected inward. This suggests the MBPG chorus waves have the potential to influence both the interior of the magnetosphere and the cusp region. Another ray path is emphasized in Figure 2e. This is the ray shown in Figure 1 and is the ray that is able to propagate to the innermost L shell. Nevertheless, this ray fails to propagate into even the extremely expanded plasmapause, which suggests the MBPG chorus waves are unlikely to propagate into the plasmasphere and contribute to plasmaspheric hiss (e.g., Bortnik et al., 2008).

Comparison between model 3 with model 1 and 2 gives similar results in terms of the localization of the wave power under average hot electron flux levels, and again shows the unlikeliness of propagation into the plasmasphere. A new finding that becomes apparent in the compressed magnetospheric model 3 compared with magnetosphere model 1, is that the rays in general propagate a shorter distance in model 3. This can be observed by comparing the termination markers between the two columns.

Figure 3 shows a summary plot of the flight time of the rays shown in Figure 2. In Figure 2, we see that there is very little difference between the first two columns. This is because magnetosphere models 1 and 2 have the same

KANG ET AL. 4 of 8



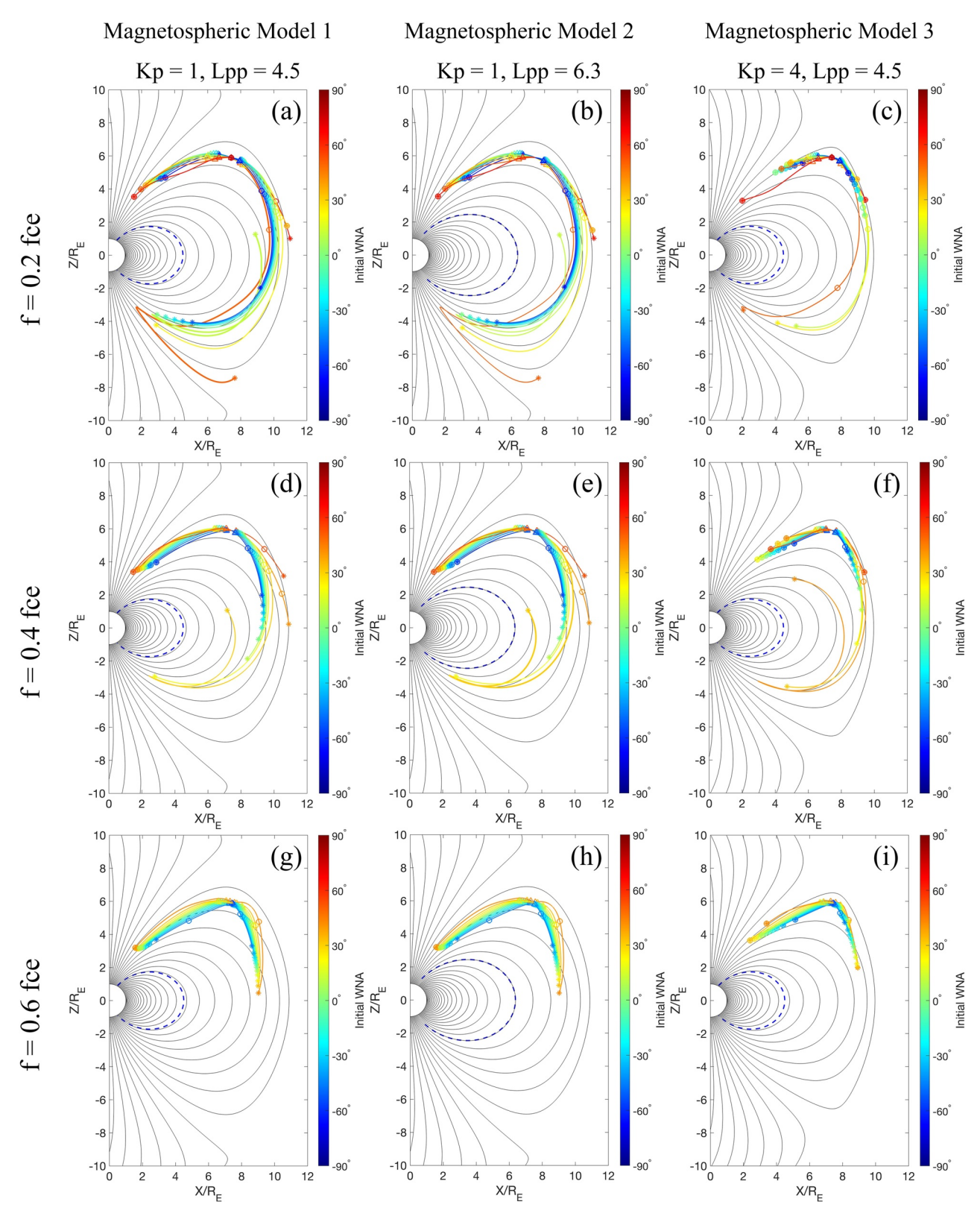


Figure 2.

KANG ET AL. 5 of 8

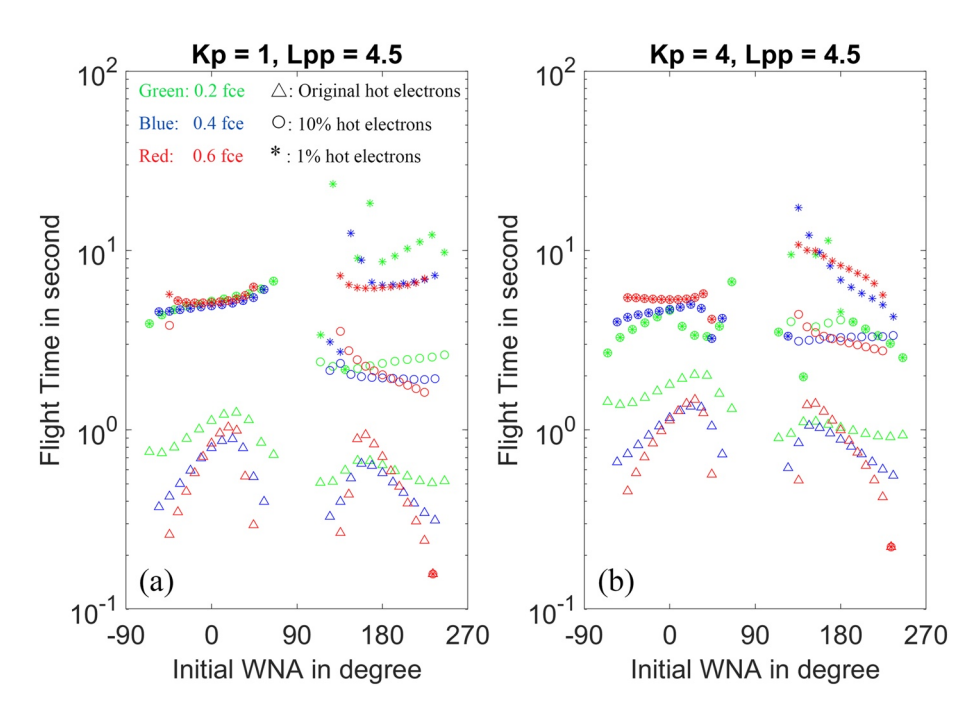


Figure 3. Summary of ray flight times. The x axis is initial WNA ranging from -90 to 270° (corresponding to the angle that initial wave vector rotates counterclockwise with respect to magnetic field). Different colors represent different frequencies. The green dots are for rays with frequency $0.2f_{ce}$, the blue ones $0.4f_{ce}$, and the red ones $0.6f_{ce}$. The shapes of the dots are for different hot electron conditions. The triangle dots are for the original hot electron distribution, the circled ones 10% hot electrons, and the starred ones 1% hot electrons. (a) is for model Kp = 1, L_{pp} = 4.5, and (b) is for model Kp = 4, L_{pp} = 6.3.

magnetic fields, and the density distributions outside the plasmapause are very similar. Since no ray goes into the plasmapause in either model, the ray tracing results are almost identical. Therefore, it is sufficient to only compare the flight time of magnetospheric models 1 and 3, which are shown in Figures 3a and 3b, respectively. The x-axis indicates the initial WNA, and the y-axis is the flight time in seconds (on a logarithmic scale). A k-vector oriented perpendicular to B and pointing away from the Earth is defined to have WNA = -90° , and the initial WNA is defined to increase counterclockwise, thus spanning a WNA ranging from -90° to 270° . Different colors of the dots represent different frequencies: the green dots for rays with $0.2 f_{ce}$, the blue dots $0.4 f_{ce}$, and the red dots $0.6 f_{ce}$. Different shapes of the dots represent different hot electron distributions: the triangle dots are for hot electron distribution of Equation 4, the circle dots 10% of Equation 4, and the star dots 1%.

In the figure, we see three bands of flight time corresponding to the three hot electron distributions, which indicates that the damping from hot electron is the main factor controlling the flight time of rays. In general, waves propagating in the +B direction toward the cusp (initial WNA -90° to 90°) would have longer flight times than those propagating in the -B direction toward the equator (initial WNA 90° to 270°). The exception is that the star dots almost all coincide with the circle dots for waves propagating in +B direction. This is because these waves are not terminated by damping, but rather by a too low phase velocity, which is independent from the hot electron distribution. Comparing Figures 3a and 3b, we see that rays under magnetospheric model 3 generally survive longer than under model 1, even though they propagate a shorter distance implying that a satellite should be able to observe these minimum-B pockets waves under more disturbed geomagnetic conditions, but only if it has the appropriate orbit.

Figure 2. Ray trajectories for three magnetospheric model. The black lines are the field lines, the blue thick dashed lines are the position of plasmapause, and the colored lines are the trajectories of rays. Different colors represent different initial WNA. Dots of different shapes on each line represent the terminating points of rays under different hot electron conditions. The triangle points are termination points for original hot electron distribution, the circled points 10% hot electrons, and the starred points 1%. (a), (d) and (g) are for model 1 (Kp = 1, L_{pp} = 4.5), (b), (e) and (h) for model 2 (Kp = 1, L_{pp} = 6.3), and (c), (f) and (i) for model 3 (Kp = 4, L_{pp} = 4.5); (a), (b) and (c) are for rays with frequency $0.2f_{ce}$, (d), (e) and (f) $0.4f_{ce}$, and (g), (h) and (i) $0.6f_{ce}$.

KANG ET AL. 6 of 8



4. Conclusion

Using our newly developed ray tracer PyRay, we conduct a ray tracing study in a non-dipole field and study the propagation of chorus waves generated from minimum-B pockets. We find that under average hot electron flux conditions, the MBPG chorus waves are highly localized in the minimum-B pockets, and hence may not be observed by spacecraft unless they are very close to the source region. Even with very low hot electron fluxes, the MBPG chorus waves are very unlikely to propagate very far, and very unlikely not as far as the plasmapause. When geomagnetic activity is stronger, the MBPG chorus waves would in general propagate a shorter distance. The ray tracing method in minimum-B geometry we propose can be further applied to future studies on electron precipitation on the outer dayside (e.g., following the method of Bortnik et al., 2016). Our study can also help identify the source region of chorus events observed by satellites on the outer dayside region, thereby improving our understanding on the global chorus waves distribution.

Data Availability Statement

The simulation data can be accessed from https://doi.org/10.5281/zenodo.5548520.

Acknowledgments References

acknowledge NASA FINESST award 80NSSC21K1393, Ning Kang, Jacob Bortnik, and S. G. Claudepierre gratefully acknowledge NSF Geospace Environment Modeling grant no. AGS-2025706, and Xin An acknowledges the support of NASA grant 80NSSC20K0917. Ning

Kang acknowledges helpful discussions

with Junyi Ren.

Ning Kang and Jacob Bortnik gratefully

Angerami, J. J., & Thomas, J. O. (1964). Studies of planetary atmospheres: 1. The distribution of electrons and ions in the Earth's exosphere. Journal of Geophysical Research, 69(21), 4537–4560. https://doi.org/10.1029/jz069i021p04537

Bortnik, J., Inan, U. S., & Bell, T. F. (2003a). Energy distribution and lifetime of magnetospherically reflecting whistlers in the plasmasphere. Journal of Geophysical Research: Space Physics 108(A5). https://doi.org/10.1029/2002ja009316

Bortnik, J., Inan, U. S., & Bell, T. F. (2003b). Frequency-time spectra of magnetospherically reflecting whistlers in the plasmasphere. *Journal of Geophysical Research: Space Physics 108*(A1). https://doi.org/10.1029/2002ja009387

Bortnik, J., Li, W., Thorne, R. M., & Angelopoulos, V. (2016). A unified approach to inner magnetospheric state prediction. *Journal of Geophysical Research: Space Physics* 121(3), 2423–2430. https://doi.org/10.1002/2015ja021733

Bortnik, J., Thorne, R. M., & Meredith, N. P. (2007). Modeling the propagation characteristics of chorus using CRRES suprathermal electron fluxes. *Journal of Geophysical Research* 112(A8). https://doi.org/10.1029/2006ja012237

Bortnik, J., Thorne, R. M., & Meredith, N. P. (2008). The unexpected origin of plasmaspheric hiss from discrete chorus emissions. *Nature* 452(7183), 62–66. https://doi.org/10.1038/nature06741

Brinca, A. L. (1972). On the stability of obliquely propagating whistlers. *Journal of Geophysical Research*, 77(19), 3495–3507. https://doi.org/10.1029/ja077i019p03495

Burtis, W. J., & Helliwell, R. A. (1969). Banded chorus—A new type of VLF radiation observed in the magnetosphere by OGO 1 and OGO 3. Journal of Geophysical Research, 74(11), 3002–3010. https://doi.org/10.1029/ja074i011p03002

Denton, R. E., Takahashi, K. I., Galkin, A., Nsumei, P. A., Huang, X., Reinisch, B. W., et al. (2006). Distribution of density along magnetospheric field lines. *Journal of Geophysical Research*, 111(A4). https://doi.org/10.1029/2005ja011414

Denton, R. E., Goldstein, J., & Menietti, J. D. (2002). Field line dependence of magnetospheric electron density. *Geophysical Research Letters*, 29(24), 58–61. https://doi.org/10.1029/2002gl015963

Golkowski, M., Harid, V., & Hosseini, P. (2019). Review of controlled excitation of non-linear wave-particle interactions in the magnetosphere. Frontiers in Astronomy and Space Sciences, 6(2).

Haselgrove, J. (1954). Ray theory and a new method for ray tracing. Proceedings of the Cambridge Conference on Physics. The Physical Society. Horne, R. B. (1989). Path-integrated growth of electrostatic waves: The generation of terrestrial myriametric radiation. Journal of Geophysical Research, 94(A7), 8895–8909. https://doi.org/10.1029/ja094ia07p08895

Horne, R. B., & Thorne, R. M. (1993). On the preferred source location for the convective amplification of ion cyclotron waves. *Journal of Geo-*

Horne, R. B., & Thorne, R. M. (2003). Relativistic electron acceleration and precipitation during resonant interactions with whistler-mode chorus. Geophysical Research Letters, 30(10). https://doi.org/10.1029/2003gl016973

Hosseini, P., Agapitov, O., Harid, V., Golkowski, M. (2021). Evidence of small scale plasma irregularity effects on whistler mode chorus propagation. *Geophysical Research Letters*, 48(5), e2021GL092850. https://doi.org/10.1029/2021gl092850

Inan, U. S., & Bell, T. F. (1977). The plasmapause as a VLF wave guide. Journal of Geophysical Research, 82(19), 2819–2827. https://doi.

org/10.1029/ja082i019p02819

Katoh, Y. (2014). A simulation study of the propagation of whistler-mode chorus in the Earth's inner magnetosphere. *Earth, Planets and Space*,

66(1), 1–12. https://doi.org/10.1186/1880-5981-66-6

Ke, Y., Chen, L., Gao, X., Lu, Q., Wang, X., Chen, R., et al. (2021). Whistler-mode waves trapped by density irregularities in the earth's magne-

tosphere. Geophysical Research Letters, 48(7), e2020GL092305. https://doi.org/10.1029/2020gl092305

Kimura, I. (1966). Effects of ions on whistler-mode ray tracing. Radio Science, 1(3), 269–284. https://doi.org/10.1002/rds196613269

LeDocq, M. J., Gurnett, D. A., & Hospodarsky, G. B. (1998). Chorus source locations from VLF Poynting flux measurements with the Polar spacecraft. Geophysical Research Letters, 25(21), 4063–4066. https://doi.org/10.1029/1998gl900071

Li, W., Thorne, R. M., Angelopoulos, V., Bortnik, J. (2009). Global distribution of whistler-mode chorus waves observed on the THEMIS spacecraft. *Geophysical Research Letters*, 36(9). https://doi.org/10.1029/2009gl037595

Li, W., Thorne, R. M., Bortnik, J., Nishimura, Y., Angelopoulos, V., Chen, L., et al. (2010). Global distributions of suprathermal electrons observed on THEMIS and potential mechanisms for access into the plasmasphere. *Journal of Geophysical Research*, 115(A12). https://doi. org/10.1029/2010ja015687

Moldwin, M. B., Downward, L., Rassoul, H. K., Amin, R., Anderson, R. (2002). A new model of the location of the plasmapause: CRRES results. Journal of Geophysical Research, 107(A11). https://doi.org/10.1029/2001ja009211

KANG ET AL. 7 of 8



- Santolík, O., Gurnett, D. A., Pickett, J. S., Parrot, M., Cornilleau Wehrlin, N. (2003). Spatio-temporal structure of storm-time chorus. *Journal of Geophysical Research*, 108(A7).
- Stix, T. H. (1992). Waves in plasmas. Springer Science & Business Media.
- Streltsov, A. V., Lampe, M., Manheimer, W. M., & Ganguli, G. (2006). Whistler propagation in inhomogeneous plasma. *Journal of Geophysical Research*, 111(A3). https://doi.org/10.1029/2005ja011357
- Summers, D., Thorne, R. M., & Xiao, F. (1998). Relativistic theory of wave-particle resonant diffusion with application to electron acceleration in the magnetosphere. *Journal of Geophysical Research*, 103(A9), 20487–20500. https://doi.org/10.1029/98ja01740
- Thorne, R. M., Li, W., Ni, B., Ma, Q., Bortnik, J., Chen, L., et al. (2013). Van Allen probe evidence of relativistic radiation belt electron acceleration by magnetospheric chorus. *Nature*, 504, 411–414. https://doi.org/10.1038/nature12889
- Tsurutani, B. T., & Smith, E. J. (1977). Two types of magnetospheric ELF chorus and their substorm dependences. *Journal of Geophysical Research*, 82(32), 5112–5128. https://doi.org/10.1029/ja082i032p05112
- Tsyganenko, N. A. (1989). A magnetospheric magnetic field model with a warped tail current sheet. *Planetary and Space Science*, 37(1), 5–20. https://doi.org/10.1016/0032-0633(89)90066-4
- Vaivads, A., Santolik, O., Stenburg, M., Andre, M., Own, P., Canu, P., et al. (2007). Source of whistler emissions at the dayside magnetopause. Geophysical Research Letters, 34(9). https://doi.org/10.1029/2006gl029195
- Xu, X., Chen, L., Zhou, C., Liu, X., Xia, Z., Simpson, J. J., et al. (2020). Two-dimensional full-wave simulation of whistler mode wave propagation near the local lower hybrid resonance frequency in a dipole field. *Journal of Geophysical Research: Space Physics*, 125(4), e2019JA027750. https://doi.org/10.1029/2019ja027750
- Yue, C., Chen, L., Bortnik, J., Ma, Q., Thorne, R. M., Angelopoulos, V., et al. (2017). The characteristic response of whistler mode waves to interplanetary shocks. *Journal of Geophysical Research: Space Physics*, 122, 10047–10057. https://doi.org/10.1002/2017ja024574

KANG ET AL. 8 of 8